Cislunar Proximity Operations in the Bi-Circular Restricted Four-Body Problem

Juan Ojeda Romero*
Johns Hopkins Applied Physics Laboratory
Fouad Khoury†
Johns Hopkins Applied Physics Laboratory

ABSTRACT

As space exploration expands past Earth orbit to the Moon and beyond, spacecraft are required to develop more capabilities in order to operate in more complex dynamical environments. Considering objectives for spacecraft rendezvous and proximity operations (RPO) in the cislunar domain, this investigation proposes and leverages a framework to characterize relative dynamics between two spacecraft in a target-chaser configuration along orbits in the Earth-Moon-Sun system described by the Bicircular Restricted Four-Body Problem (BCRFBP). First, a novel parameterization of the relative dynamics is introduced and numerically validated along two non-Keplerian reference orbits in the BCRFBP. The resulting equations of motion are linearized about the target spacecraft's position and implemented as elements of a multiple-shooting strategy that enable the ability to design relative trajectories in a Local-Vertical-Local-Horizontal (LVLH) frame attached to the target's center. Two RPO demonstrations involving the target-chaser configuration are simulated along the reference orbits which include a 9:2 L_2 Near Rectilinear Halo Orbit (NRHO) and a 3:1 L_1 Northern Halo orbit. In each demonstration, the chaser achieves a successful rendezvous with the target spacecraft while adhering to specific Sun-lit geometries during its close approach. The results of this investigation underscore the benefit of characterizing spacecraft relative dynamics in the BCRFBP to model rendezvous and proximity operations in a multibody gravitational environment.

1. INTRODUCTION

As NASA moves to enable a more permanent human presence beyond Earth orbit, a need arises to further develop the current state-of-the-art in spacecraft guidance, navigation, and control (GNC) technologies with the aim of operating in more challenging dynamical environments. Notably, NASA's Artemis program seeks a return to the Moon in order to leverage the lunar surface and surrounding cislunar region as a proving ground to test new technologies for coordinating spacecraft to meet near and long term human exploration objectives. For example, NASA's

*Mission Design Engineer, Space Exploration Sector, John Hopkins University Applied Physics Laboratory, 11100 John Hopkins Road, Office 200-W540, Laurel, MD 20723. Juan.Ojeda.Romero@jhuapl.edu

†Mission Design and Navigation Engineer, Space Exploration Sector, John Hopkins University Applied Physics Laboratory, 11100 John Hopkins Road, Office 200-W540, Laurel, MD 20723. Fouad.Khoury@jhuapl.edu

Copyright © 2023 Advanced Maui Optical and Space Surveillance Technologies Conference (AMOS) – www.amostech.com

proposed orbiting platform Gateway, slated to be the first deep-space station beyond low Earth orbit, is expected to orbit near the Moon in a 9:2 Lunar Synodic Resonant Near Rectilinear Halo Orbit (NRHO) to serve as a staging location for missions to the lunar surface and beyond.[19] A critical element of these future space architectures warrant the capability to coordinate multiple spacecraft relative to one another in order to accomplish mission objectives such as rendezvous and proximity operations. As a result, the need arises to advance relative motion GNC technologies and design strategies in flight regimes simultaneously governed by multiple gravitational influences from the Moon, Earth, and Sun.

Most of the previous work in relative motion modeling has been confined to near-Keplerian orbit regimes where the gravitational influence on spacecraft is assumed to stem from a single primary body with the inclusion of additional perturbations as first-order approximations of the corresponding force model.[16] Among the earliest relative motion dynamics models developed include the Hill-Clohessy-Wiltshire (HCW) equations which were formulated to model rendezvous operations in low Earth orbit.[6] These equations characterize the relative motion of a chaser spacecraft with respect to a target spacecraft in a circular orbit around a single gravitational primary. The HCW model fails to characterize the relative dynamics if the target spacecraft's orbit is eccentric or the chaser spacecraft's relative state exceeds more than 20 km.[16] The Yamanaka-Ankersen model improves upon this limitation by characterizing relative motion in target-chaser configurations along highly eccentric orbits.[18] Schaub et al. further developed relative motion models that utilize differences in orbit elements to incorporate additional perturbations including J_2 Earth gravity harmonics.[14] Similarly, Sullivan, Grimberg, and D'Amico employ a dynamical formulation based on relative orbital elements (ROEs) to characterize relative motion under additional perturbing accelerations including solar radiation pressure and three-body effects.[16] Although each of the abovementioned relative motion models has been validated extensively in their applicable flight regimes, they employ the underlying assumption that the governing relative dynamics are mostly Keplerian. Additional perturbing accelerations are approximated using first-order series expansions of the force model descriptions and assumed to be minor perturbations in comparison to the purely Keplerian description of the orbital motion. Consequently, these models fail to adequately characterize the relative spacecraft dynamics in flight regimes with more than one gravitational primary including the cislunar environment.[11]

More recently, relative motion in more complex dynamical regimes, like the Circular Restricted Three-Body Problem (CRTBP) model, has been investigated. Franzini et al. initially developed nonlinear equations of relative motion relative to a target spacecraft's LVLH frame in the CRTBP for rendezvous applications along orbits close to the lunar vicinity.[7] Khoury & Lippe further develop the relative equations of motion by establishing the Moon, L_1, and L_2 as "anchor points" that define the target LVLH frame geometry for orbits residing further away from the Moon's near vicinity and close to the Earth-Moon libration points.[10] In their work, Khoury & Lippe formulate multiple shooting strategies to demonstrate orbital rendezvous and spacecraft loitering along a variety of orbits defined in the CRTBP. Moreover, they implement the different geometric configurations of the target's LVLH frame in a relative navigation filter to demonstrate tracking between spacecraft using simulated on-board bearing angle and range measurements. Although these abovementioned dynamical models are improvements from their Keplerian-based counterparts, they still ignore the nontrivial influence of the Sun on certain trajectories in the cislunar environment.

Copyright © 2023 Advanced Maui Optical and Space Surveillance Technologies Conference (AMOS) – www.amostech.com

To incorporate the Sun's influence, this investigation leverages an extension of the CRTBP model, i.e., the Bicircular Restricted Four-Body Problem (BCRFBP) model. Insights from the BCRFBP model have been successfully implemented in preliminary mission design studies and have been used to explore the complex dynamics in cislunar space. Boudad et. al[3,4] investigated disposal strategies from the 9:2 L_2 NRHO within the BCRFBP model and the high-fidelity ephemeris force model. Additionally, multiple authors have leveraged the Sun's influence to construct low-energy Ballistic Lunar Transfers (BLTs) to a range of regions within cislunar space.[2,12,13,15] The implementation of lower fidelity dynamical models which describe the Sun-Earth-Moon system facilitates the construction of feasible relative motion transfers for rendezvous and proximity operations in cislunar space.

This investigation proposes a novel framework to construct rendezvous and proximity operations (RPO) scenarios between a target and chaser spacecraft within the BCRFBP model. The structure of this paper is as follows; First, the BCRFBP model is defined as an extension to the CRTBP model which incorporates the Sun's gravitational influence. A set of nonlinear relative equations of motion (EOMs) characterizing a chaser's motion relative to a target spacecraft are derived based on the dynamics of the BCRFBP model. Next, a set of linearized EOMs corresponding to the relative BCRFBP EOMs are derived and validated along the selected 9:2 L_2 NRHO and 3:1 southern L_1 halo orbit. Two rendezvous and proximity operations scenarios are evaluated and examined along each reference orbit. First, a target-chaser spacecraft configuration is used to describe a possible rendezvous scenario between NASA's Gateway orbiting platform and the Orion spacecraft along a 9:2 L_2 NRHO. The chaser's close approach and resulting rendezvous trajectory is constrained to adhere to a desired solar geometry relative to the target to demonstrate Orion's close approach to Gateway in a sun lit region of the NRHO. Secondly, a low-energy BLT is constructed to insert along a lunar synodic resonant 3:1 L_1 southern halo orbit within the BCRFBP model. Upon insertion, the chaser spacecraft performs a number of maneuvers relative to the target spacecraft with the objective of achieving terminal rendezvous within some specified time of flight (TOF). The main contributions of this paper are summarized as follows: First, relative EOMs are derived from the BCRFBP model for a target and chaser configuration. Second, a validation analysis is performed based on the linearized relative EOMs for the set of selected cislunar orbits. Finally, two rendezvous and proximity scenarios along the selected reference orbits are considered to demonstrate a feasible preliminary design within the dynamical framework of the relative motion BCRFBP model.

2. DYNAMICS

2.1 Bicircular Restricted Four-Body Problem

Key elements of NASA's proposed architectures for the upcoming Artemis missions include orbits that arise when gravitational accelerations from both the Earth and Moon are incorporated simultaneously. Moreover, some mission requirements, including those pertaining to NASA's proposed rendezvous and proximity operations between Orion and Gateway, stipulate that Orion's close approach be performed while adhering to specific solar geometries with respect to Gateway along its orbit. The BCRFBP is a lower-fidelity model that incorporates the gravitational influence of all three celestial bodies within one dynamical framework.[9] In the Sun-Earth-Moon, SEM, system, the model is derived in either the Earth-Moon rotating frame or the Sun-B_1 rotating frame,

Copyright © 2023 Advanced Maui Optical and Space Surveillance Technologies Conference (AMOS) – www.amostech.com

where B_1 is the Earth-Moon barycenter. The SEM BCRFBP model is an extension of the Earth-Moon CRTBP model with the inclusion of the Sun's gravitational influence. Figure 1(a) describes the Earth-Moon rotating frame of the BCRFBP model consistent with the rotating frame of the CRTBP model. Note that the Sun moves in a clockwise direction with respect to the Earth-Moon barycenter, B_1. Moreover, the BCRFBP stipulates that the positions of the Earth and the Moon

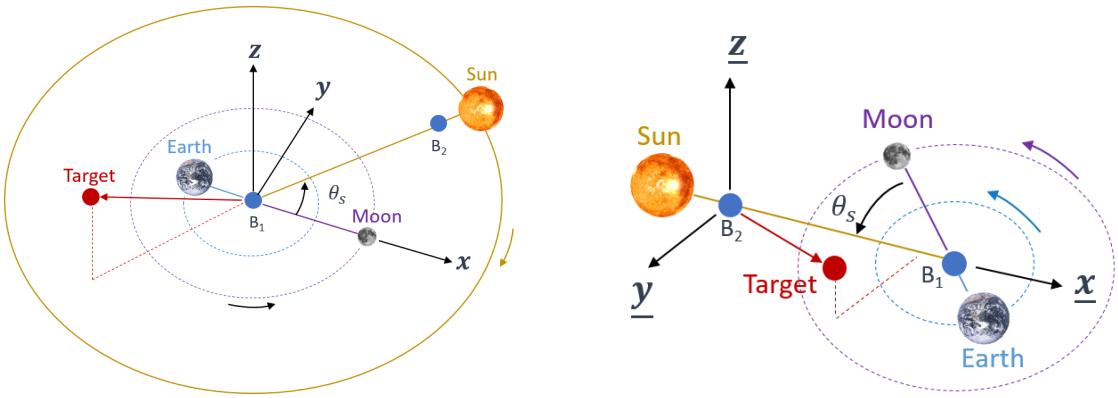

(a) (b)

Fig. 1: (a) Earth-Moon rotating frame of the BCRFBP model. (b) Sun-B_1 rotating frame of the BCRFBP model. The origin is the Sun-Earth-Moon barycenter, B_2. Figures adapted from Boudad[3]

are fixed in the Earth-Moon rotating frame. For consistency with previous authors, the EOMs for the BCRFBP model are non-dimensionalized with a characteristic length, l^*, and a characteristic time, t^*, see Boudad[4] for common definitions of the characteristic values. In Fig. 1(a), the Earth-Moon rotating frame of the BCRFBP is defined via the following set of vectors $\{\hat{\mathbf{x}}, \hat{\mathbf{y}}, \hat{\mathbf{z}}\}$ where, $\hat{\mathbf{x}}$ points from the Earth to the Moon, $\hat{\mathbf{z}}$ is in the direction of the Moon's angular momentum, and $\hat{\mathbf{y}}$ completes the right-handed triad. In this investigation, vectors are expressed in lower-case bold text and matrices are written in upper-case bold text. A gravitational mass parameter, μ, is introduced and is defined as: $\mu = \frac{m_2}{m_1+m_2}$, where m_1 and m_2 corresponds to the mass of the Earth and Moon, respectively. From Fig. 1(a), the position of the sun in the Earth-Moon rotating frame is,

$$\mathbf{r}_s = [a_s \cos(\theta_s), a_s \sin(\theta_s), 0], \tag{1}$$

where a_s is the nondimensionalized distance of the Sun relative to the Earth-Moon barycenter, B_1, and θ_s is the Sun angle measured from the $\hat{\mathbf{x}}$ axis. The EOMs for the BCR4BP model are written as,

$$\ddot{x} - 2\dot{y} = \frac{\partial \Gamma}{\partial x}, \tag{2}$$

$$\ddot{y} + 2\dot{x} = \frac{\partial \Gamma}{\partial y}, \tag{3}$$

$$\ddot{z} = \frac{\partial \Gamma}{\partial z}, \tag{4}$$

Copyright © 2023 Advanced Maui Optical and Space Surveillance Technologies Conference (AMOS) – www.amostech.com

where Γ is the pseudo-potential corresponding to the model expressed as ,

$$\Gamma = \frac{1}{2}(x^2 + y^2) + \frac{(1-\mu)}{r_{et}} + \frac{\mu}{r_{mt}} + \frac{\mu_s}{r_{st}} - \frac{\mu_s}{a_s^3}(\mathbf{r}_s \cdot \mathbf{r}), \tag{5}$$

where μ_s denotes the mass of the Sun non-dimensionalized using the combined mass of the Earth and Moon, m^*. The vectors $\mathbf{r}_{et}$, $\mathbf{r}_{mt}$, and $\mathbf{r}_{st}$ correspond to the spacecraft's position measured relative to the Earth, Moon, and Sun, respectively. Additionally, the EOMs for the BCRFBP model are also derived in a Sun-B_1 rotating frame where the origin coincides at the barycenter of the Sun-Earth-Moon system and the corresponding EOMs are described via the vector set $\{\hat{\underline{\mathbf{x}}}, \hat{\underline{\mathbf{y}}}, \hat{\underline{\mathbf{z}}}\}$, see Fig. 1(b). The derivation of the EOMs is presented by Boudad,[4] McCarthy,[12] and Huang.[9] Note that the dynamics of the BCRFBP model is the same in both the Earth-Moon and Sun-B_1 frames. Although the BCRFBP model is not coherent, e.g., the motion of the Earth, Moon, and Sun are assumed to be along the same orbital plane, it offers an intermediate fidelity representation of the complex dynamics of the system before transitioning to the higher-fidelity ephemeris force model.[9]

2.1.1 Orbit Selection in the BCRFBP model

Periodic motion observed in a dynamical model provides insightful properties that facilitate the construction of complex cislunar transfers. Within the context of the CRTBP model, periodic orbits exist as members of families of periodic orbits.[17] Recall that the BCRFBP model is an extension of the CRTBP model where the gravitational influence of the fourth body where the Sun is represented as a periodic perturbation. In the BCRFBP model, periodic orbits exist as isolated solutions that are resonant with the synodic period of the model, e.g., 29.5 days in the Earth-Moon-Sun system. Multiple authors have successfully implemented numerical methods to compute periodic orbits in the BCRFBP model from an initial CRTBP periodic orbit. Boudad et. al. implemented a natural parameter continuation technique based on a homotopy method which slowly increased the Sun's gravity by introducing a scaling factor to the Sun's mass, μ_s in Eq. 5. This investigation explores transfers and proximity operations near two candidate orbits: a 3:1 L_1 southern halo orbit and a 9:2 L_2 NRHO (the selected orbit for the Gateway mission[19]). Note that the 3:1 L_1 halo corresponds to three revolutions along the orbit per one synodic period and the 9:2 L_2 NRHO represents nine revolutions for two synodic periods. The candidate orbits are constructed by implementing a pseudo-arclength continuation method consistent with previous authors.[4,12] Figure 2 presents the selected orbits in the Earth-Moon and Sun-B_1 frames, note that the colors in Figure 2 represent the associated sun angle, θ_s, over time.

Copyright © 2023 Advanced Maui Optical and Space Surveillance Technologies Conference (AMOS) – www.amostech.com

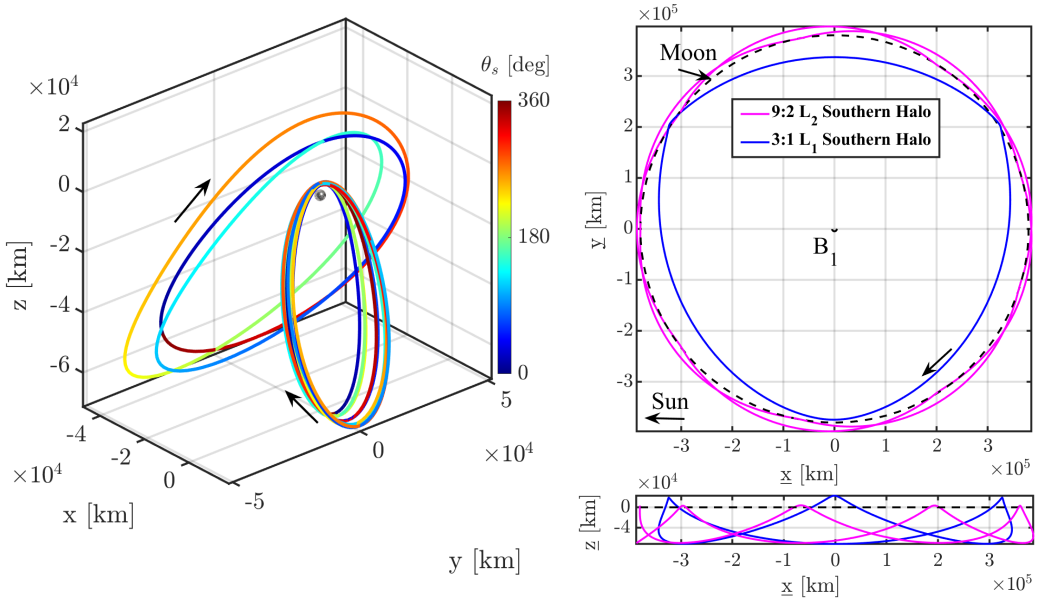

(a) (b)

Fig. 2: (a) Candidate orbits in the Moon-centered Earth-Moon frame. The color corresponds to the sun angle. (b) Candidate orbits in the B_1-centered Sun-B_1 frame. The Moon is represented in the dashed line

2.2 Relative Equations of Motion in the BCRFBP

In this section, a formulation is presented to characterize the relative dynamics between spacecraft in a target-chaser configuration subject to the gravitational influence of the Earth, Moon, and Sun as point masses. The relative dynamics involves the propagation of four separate elements; namely, the target spacecraft's absolute state in the Earth-Moon rotating frame, the kinematic expressions governing the target spacecraft's LVLH frame over time, the chaser's relative state with respect to the target, and finally the Sun's angle with respect to the Earth-Moon system. All of the corresponding equations belonging to each of these four elements are propagated simultaneously providing full state knowledge of both spacecraft and the system dynamics for a specified time interval. As a result, a geometrically intuitive model of the relative dynamics is obtained and used to describe target-chaser configurations along orbits defined in the BCRFBP.

As described in Franzini et al.[7] and Khoury & Lippe,[10] the nonlinear equations of relative motion for a chaser spacecraft with respect to a target spacecraft in the CRTBP are formulated in the target's LVLH frame. In order to formulate the nonlinear equations of relative motion in the BCRFBP, the gravitational force due to the Sun is incorporated as an additional acceleration

Copyright © 2023 Advanced Maui Optical and Space Surveillance Technologies Conference (AMOS) – www.amostech.com

imparted on both spacecraft. Consequently, the relative equations of motion can be written as

$$[\underset{T}{\ddot{\boldsymbol{\rho}}}] = -2\boldsymbol{\omega}_{T/I} \times [\underset{T}{\dot{\boldsymbol{\rho}}}] - [\underset{T}{\dot{\boldsymbol{\omega}}_{T/I}}] \times \boldsymbol{\rho} - \boldsymbol{\omega}_{T/I} \times (\boldsymbol{\omega}_{T/I} \times \boldsymbol{\rho}) \tag{6}$$
$$+\mu\left(\frac{\boldsymbol{r}}{r^3} - \frac{\boldsymbol{r}+\boldsymbol{\rho}}{||\boldsymbol{r}+\boldsymbol{\rho}||^3}\right) + (1-\mu)\left(\frac{\boldsymbol{r}+\vec{r}_{em}}{||\boldsymbol{r}+\boldsymbol{r}_{em}||^3} - \frac{\boldsymbol{r}+\boldsymbol{\rho}+\boldsymbol{r}_{em}}{||\boldsymbol{r}+\boldsymbol{\rho}+\boldsymbol{r}_{em}||^3}\right) + \mu_s\left(\frac{\boldsymbol{r}+\boldsymbol{r}_{sm}}{||\boldsymbol{r}+\boldsymbol{r}_{sm}||^3} - \frac{\boldsymbol{r}+\boldsymbol{\rho}+\boldsymbol{r}_{sm}}{||\boldsymbol{r}+\boldsymbol{\rho}+\boldsymbol{r}_{sm}||^3}\right)$$

where the terms following the Sun gravitational parameter μ_s supplement the CRTBP relative equations of motion by incorporating the Sun's acceleration in the BCRFBP. In this formulation, $\boldsymbol{r}$ is the target's position vector relative to the Moon and $\boldsymbol{\rho}$ is the relative position vector measured from the target to the chaser. Moreover, $\boldsymbol{r}_{em}$ and $\boldsymbol{r}_{sm}$ refer to the Moon's position vector relative to the Earth and Sun, respectively, with their corresponding norms denoted as r_{em} and r_{sm}. The Sun's position with respect to the Earth-Moon system is computed using the Sun angle θ_s in the BCRFBP model. The target spacecraft's LVLH frame is denoted as T with the surrounding brackets (i.e. $[\underset{T}{\dot{\boldsymbol{\rho}}}]$) indicating that derivatives are taken in the frame specified by the subscript. The quantities $\boldsymbol{\omega}_{T/I}$ and $[\underset{T}{\dot{\boldsymbol{\omega}}_{T/I}}]$ correspond to the angular velocity and angular acceleration of the LVLH frame T with respect to an inertial frame I, respectively.

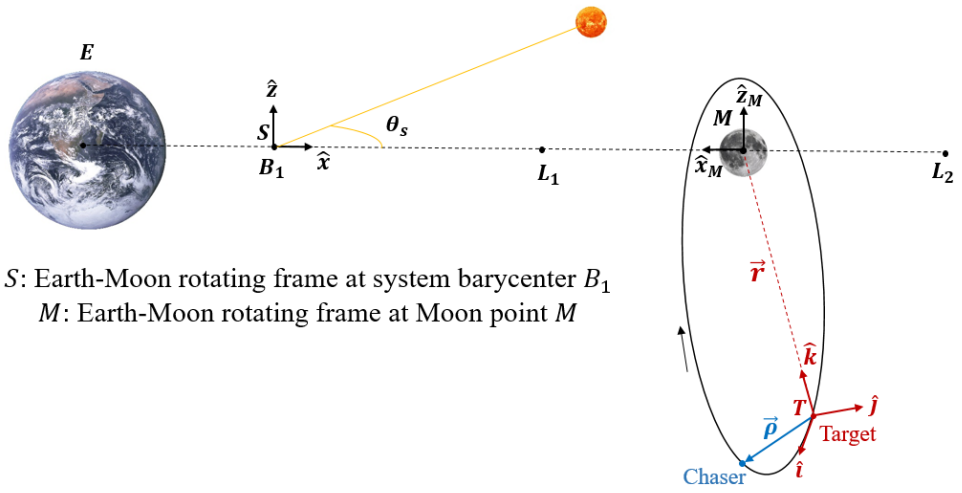

S: Earth-Moon rotating frame at system barycenter B_1
M: Earth-Moon rotating frame at Moon point M

Fig. 3: Schematic of a target-chaser configuration in the BCRFBP. The target's LVLH frame T (red) is formulated using the target's absolute state vector relative to the Earth-Moon rotating frame M originating at the Moon's center.

The kinematic expressions governing the time evolution of the LVLH frame, $\boldsymbol{\omega}_{T/I}$ and $[\underset{T}{\dot{\boldsymbol{\omega}}_{T/I}}]$, are functions of the target spacecraft's state in the Earth-Moon rotating frame. For example, the angular velocity of the LVLH frame T is the summation of two other components expressed as:

$$\boldsymbol{\omega}_{T/I} = \boldsymbol{\omega}_{T/M} + \boldsymbol{\omega}_{M/I} \tag{7}$$

where $\boldsymbol{\omega}_{M/I}$ denotes the angular velocity of an Earth-Moon rotating frame based at the Moon's center, denoted as M, with respect to an inertial frame I and $\boldsymbol{\omega}_{T/M}$ denotes the angular velocity of

Copyright © 2023 Advanced Maui Optical and Space Surveillance Technologies Conference (AMOS) – www.amostech.com

the target spacecraft's LVLH frame T with respect to the Earth-Moon rotating frame M. As depicted in Figure 3, frame M coincides with the location of the Moon's center along the Earth-Moon line with $\hat{\mathbf{x}}_M$ axis pointing towards the Earth, $\hat{\mathbf{z}}_M$ parallel to the Moon's angular momentum vector, and $\hat{\mathbf{y}}_M = \hat{\mathbf{z}}_M \times \hat{\mathbf{x}}_M$ pointing out of the page. This axis configuration mirrors the conventional BCRFBP Earth-Moon synodic frame S, conventionally originating at the system barycenter B, but is placed at the Moon's center for convenience. Consequently, the propagation of the target spacecraft's dynamics in the BCRFBP yields state information relative to the Moon's center in frame M. Additionally, the BCRFBP stipulates that the Moon orbits the Earth at a constant angular rate, thus $\boldsymbol{\omega}_{M/I} = 1\hat{\mathbf{z}}_M$. Separately, $\boldsymbol{\omega}_{T/M}$ is kinematically expressed in terms of the absolute state of the target spacecraft relative to the Moon. As depicted in Figure 3, the target spacecraft's position and velocity vectors, denoted as $\boldsymbol{r}$ and $[\underset{M}{\dot{\boldsymbol{r}}}]$, respectively, define LVLH frame T such that:

$$\hat{\mathbf{i}} = \hat{\mathbf{j}} \times \hat{\mathbf{k}} \qquad \hat{\mathbf{j}} = -\frac{\boldsymbol{r} \times [\underset{M}{\dot{\boldsymbol{r}}}]}{||\boldsymbol{r} \times [\underset{M}{\dot{\boldsymbol{r}}}]||} \qquad \hat{\mathbf{k}} = -\frac{\boldsymbol{r}}{r} \tag{8}$$

The axes $\hat{\mathbf{i}}$, $\hat{\mathbf{j}}$, and $\hat{\mathbf{k}}$, analogous to the conventional V-bar, H-bar, and R bar axes used for Earth-orbiting relative motion applications, constitute the rotating LVLH reference frame T anchored at the target spacecraft. The angular velocity vector $\boldsymbol{\omega}_{T/M}$ can then be expressed in terms of LVLH components as

$$\boldsymbol{\omega}_{T/M} = \omega^y_{T/M}\hat{\mathbf{j}} + \omega^z_{T/M}\hat{\mathbf{k}} \tag{9}$$

Similarly, the angular acceleration of the target's LVLH frame is expressed as:

$$[\underset{T}{\dot{\boldsymbol{\omega}}_{T/I}}] = [\underset{T}{\dot{\boldsymbol{\omega}}_{T/M}}] + [\underset{T}{\dot{\boldsymbol{\omega}}_{M/I}}] = [\underset{T}{\dot{\boldsymbol{\omega}}_{T/M}}] - \boldsymbol{\omega}_{T/M} \times \vec{\boldsymbol{\omega}}_{M/I} \tag{10}$$

with the angular acceleration vector of the LVLH frame T with respect to the Earth-Moon rotating frame M written in component-wise form as

$$[\underset{T}{\dot{\boldsymbol{\omega}}_{T/M}}] = \dot{\omega}^y_{T/M}\hat{\mathbf{j}} + \dot{\omega}^z_{T/M}\hat{\mathbf{k}} \tag{11}$$

The kinematic equations for each of the components of $\boldsymbol{\omega}_{T/M}$ and $[\underset{T}{\dot{\boldsymbol{\omega}}_{T/M}}]$ are identical to expressions given in Franzini et al.[7] and Khoury & Lippe[10] except for the computation of the target spacecraft's acceleration and jerk vectors which must be adjusted to account for the Sun's gravitational acceleration. Therefore, the LVLH frame kinematics are written as

$$\omega^y_{T/M} = \frac{h}{r^2} \qquad \omega^z_{T/M} = -\frac{r}{h^2}\boldsymbol{h} \cdot [\underset{M}{\ddot{\boldsymbol{r}}}] \tag{12}$$

$$\dot{\omega}^y_{T/M} = -\frac{1}{r}\left(\frac{\dot{h}}{r} + 2\dot{r}\omega^y_{T/M}\right) \qquad \dot{\omega}^z_{T/M} = \left(\frac{\dot{r}}{r} - 2\frac{\dot{h}}{h}\right)\omega^z_{T/M} - \frac{r}{h^2}\boldsymbol{h} \cdot [\underset{M}{\dddot{\boldsymbol{r}}}] \tag{13}$$

where

$$h = |\boldsymbol{r} \times [\underset{M}{\dot{\boldsymbol{r}}}]| \qquad \dot{r} = \frac{1}{r}\boldsymbol{r} \cdot [\underset{M}{\dot{\boldsymbol{r}}}] \qquad [\underset{M}{\dot{\boldsymbol{h}}}] = \boldsymbol{r} \times [\underset{M}{\ddot{\boldsymbol{r}}}] \qquad \dot{h} = -[\underset{M}{\dot{\boldsymbol{h}}}] \cdot \hat{\mathbf{j}} \tag{14}$$

Copyright © 2023 Advanced Maui Optical and Space Surveillance Technologies Conference (AMOS) – www.amostech.com

with the target spacecraft's acceleration vector computed as

$$[\underset{M}{\ddot{\boldsymbol{r}}}] = -2\boldsymbol{\omega}_{M/I} \times [\underset{M}{\dot{\boldsymbol{r}}}] - \boldsymbol{\omega}_{M/I} \times (\boldsymbol{\omega}_{M/I} \times \boldsymbol{r}) - \mu \frac{\boldsymbol{r}}{r^3} - (1-\mu)\left(\frac{\boldsymbol{r}+\boldsymbol{r}_{em}}{||\boldsymbol{r}+\boldsymbol{r}_{em}||^3} - \frac{\boldsymbol{r}_{em}}{r_{em}^3}\right) - \mu_s\left(\frac{\boldsymbol{r}+\boldsymbol{r}_{sm}}{||\boldsymbol{r}+\boldsymbol{r}_{sm}||^3} - \frac{\boldsymbol{r}_{sB}}{r_{sB}^3}\right) \tag{15}$$

and the target's jerk vector computed as

$$\begin{aligned}[\underset{M}{\dddot{\boldsymbol{r}}}] = &-2\boldsymbol{\omega}_{M/I} \times [\underset{M}{\ddot{\boldsymbol{r}}}] - \boldsymbol{\omega}_{M/I} \times (\boldsymbol{\omega}_{M/I} \times [\underset{M}{\dot{\boldsymbol{r}}}]) - \mu \frac{\partial}{\partial \boldsymbol{r}}\left[\frac{\boldsymbol{r}}{r^3}\right][\underset{M}{\dot{\boldsymbol{r}}}] - (1-\mu)\frac{\partial}{\partial \boldsymbol{r}}\left[\frac{\boldsymbol{r}+\boldsymbol{r}_{em}}{||\boldsymbol{r}+\boldsymbol{r}_{em}||^3}\right][\underset{M}{\dot{\boldsymbol{r}}}] \\ &- \mu_s \frac{\partial}{\partial \boldsymbol{r}}\left[\frac{\boldsymbol{r}+\boldsymbol{r}_{sm}}{||\boldsymbol{r}+\boldsymbol{r}_{sm}||^3}\right]([\underset{M}{\dot{\boldsymbol{r}}}] + [\underset{M}{\dot{\boldsymbol{r}}_{sm}}]) + \mu_s \frac{\partial}{\partial \boldsymbol{r}}\left[\frac{\boldsymbol{r}_{sB}}{||\boldsymbol{r}_{sB}||^3}\right][\underset{M}{\dot{\boldsymbol{r}}_{sB}}]\end{aligned} \tag{16}$$

where it follows that for any vector $\boldsymbol{\xi}$,

$$\frac{\partial}{\partial \boldsymbol{\xi}}\left[\frac{\boldsymbol{\xi}}{\xi^3}\right] = \frac{1}{\xi^3}\left(\mathbf{I}_{3x3} - 3\frac{\boldsymbol{\xi}\boldsymbol{\xi}^T}{\xi^2}\right)$$

Equation (15-16) denote the acceleration and jerk of the target spacecraft in the BCRFBP with respect to frame M, respectively. The vector $\boldsymbol{r}_{sB}$ denotes the position vector of the Earth-Moon barycenter relative to the Sun which is a function of Sun angle θ_S. Note that due to the definition of the LVLH frame, the angular velocity and acceleration along the $\hat{\mathbf{i}}$ direction is zero. Therefore, the computation of both angular velocity components $\omega_{T/M}^{y}$ and $\omega_{T/M}^{z}$ (specified as the *orbit rate* and the *steering rate*, respectively) and their corresponding derivatives govern the dynamics of the target spacecraft's LVLH frame in time.

2.3 Linearization of Relative Equations of Motion

The nonlinear relative equations of motion are further simplified by linearizing the gravitational accelerations around the target spacecraft's position along the reference orbit. Consider a chaser's position relative to the target spacecraft which can be written as

$$\boldsymbol{r}_c = \boldsymbol{r} + \boldsymbol{\rho}. \tag{17}$$

The gravitational acceleration on the chaser spacecraft due to the three gravitational primaries are expressed as

$$\boldsymbol{g}_m(\boldsymbol{r}_c) = -\mu\frac{\boldsymbol{r}_c}{r_c^3} \qquad \boldsymbol{g}_e(\boldsymbol{r}_c+\boldsymbol{r}_{em}) = -(1-\mu)\frac{\boldsymbol{r}_c+\boldsymbol{r}_{em}}{||\boldsymbol{r}_c+\boldsymbol{r}_{em}||^3} \qquad \boldsymbol{g}_s(\boldsymbol{r}_c+\boldsymbol{r}_{sm}) = -\mu_s\frac{\boldsymbol{r}_c+\boldsymbol{r}_{sm}}{||\boldsymbol{r}_c+\boldsymbol{r}_{sm}||^3} \tag{18}$$

where $\boldsymbol{g}_m$, $\boldsymbol{g}_e$, and $\boldsymbol{g}_s$ denote the gravitational accelerations on the chaser spacecraft due to the Moon, Earth, and Sun, respectively. A first order Taylor series expansion applied around the target spacecraft's position yields approximate expressions for the chaser spacecraft's acceleration in the BCRFBP. As a result, the linear equations of relative motion are obtained and written as

$$\begin{aligned}[\underset{T}{\ddot{\boldsymbol{\rho}}}] = &-2\boldsymbol{\Omega}_{T/I}[\underset{T}{\dot{\boldsymbol{\rho}}}] - \left([\underset{T}{\dot{\boldsymbol{\Omega}}_{T/I}}] + \boldsymbol{\Omega}_{T/I}^2 + \frac{\mu}{r^3}\left(\mathbf{I} - 3\frac{\boldsymbol{r}\boldsymbol{r}^T}{r^2}\right)\right. \\ &\left. + \frac{1-\mu}{||\boldsymbol{r}+\boldsymbol{r}_{em}||^3}\left(\mathbf{I} - 3\frac{(\boldsymbol{r}+\boldsymbol{r}_{em})(\boldsymbol{r}+\boldsymbol{r}_{em})^T}{||\boldsymbol{r}+\boldsymbol{r}_{em}||^2}\right) + \frac{\mu_s}{||\boldsymbol{r}+\boldsymbol{r}_{sm}||^3}\left(\mathbf{I} - 3\frac{(\boldsymbol{r}+\boldsymbol{r}_{sm})(\boldsymbol{r}+\boldsymbol{r}_{sm})^T}{||\boldsymbol{r}+\boldsymbol{r}_{sm}||^2}\right)\right)\boldsymbol{\rho}\end{aligned} \tag{19}$$

Copyright © 2023 Advanced Maui Optical and Space Surveillance Technologies Conference (AMOS) – www.amostech.com

where $\mathbf{\Omega}_{T/I}$ and $[\underset{T}{\dot{\mathbf{\Omega}}_{T/I}}]$ are skew symmetric matrices that contain the LVLH components of the angular velocity and acceleration vectors, $\boldsymbol{\omega}_{T/I}$ and $[\underset{T}{\dot{\boldsymbol{\omega}}_{T/I}}]$, such that

$$\mathbf{\Omega}_{T/I} = \begin{bmatrix} 0 & -\omega^z_{T/I} & \omega^y_{T/I} \\ \omega^z_{T/I} & 0 & -\omega^x_{T/I} \\ -\omega^y_{T/I} & \omega^x_{T/I} & 0 \end{bmatrix} \qquad [\underset{T}{\dot{\mathbf{\Omega}}_{T/I}}] = \begin{bmatrix} 0 & -\dot{\omega}^z_{T/I} & \dot{\omega}^y_{T/I} \\ \dot{\omega}^z_{T/I} & 0 & -\dot{\omega}^x_{T/I} \\ -\dot{\omega}^y_{T/I} & \dot{\omega}^x_{T/I} & 0 \end{bmatrix} \tag{20}$$

2.3.1 Linearized Model Accuracy

In order to evaluate the accuracy of the linearized relative motion models, numerical integration of the corresponding equations of motion are performed along both reference orbits. The linear equations of relative motion, expressed in Equation 19, are propagated along a 9:2 L_2 Near Rectilinear Halo Orbit (NRHO) and a 3:1 L_1 southern halo orbit in the BCRFBP. After propagating the EOMs for a specified time interval, the approximations provided by the linearized model are compared against the results stemming from the propagation of the corresponding nonlinear equations of relative motion, expressed in Equation 6. The accuracy results demonstrate the limits of the first-order linear assumptions along each reference orbit to identify locations best suited for proximity operations between the spacecraft.

Two numerical simulations are carried out in MATLAB using the ode113 differential solver with a absolute and relative tolerance of 1×10^{-13}. In both simulations, a target spacecraft is placed at different points along its corresponding reference orbit. To specify the target's initial position, a mean anomaly parameter, Ψ_T, is defined such that

$$\Psi_T = 2\pi \frac{(t - t_0)}{P} \tag{21}$$

where $(t - t_0)$ denotes the time elapsed since some initial epoch on the reference orbit, Ψ_0, and P is time needed for target to complete one revolution. Since the periods of the reference orbits are commensurate with the synodic period of the Earth-Moon-Sun system, the time it takes the target to complete one revolution is equivalent to the time between perilunes. Next, a number of fictitious "chaser" spacecraft are initialized both ahead ($+\hat{\mathbf{i}}$) and behind ($-\hat{\mathbf{i}}$) the target spacecraft's initial position along its LVLH reference frame. Similarly, the positions of the chaser spacecraft relative to the target can also be parameterized by a quantity $\Delta\Psi$ described as

$$\Delta\Psi = \Psi_C - \Psi_T \tag{22}$$

where Ψ_C denotes the mean anomaly of the chaser along the target's reference orbit. Once the relative states between the spacecraft are initialized, they are propagated using both the linearized relative motion dynamics and nonlinear equations of motion for a specified TOF. The relative state approximations resulting from the linearized model are compared to the results of the nonlinear equations, established as truth, and evaluated using a performance index defined such that

$$e_p = \max_{t \in [0 \text{ TOF}]} ||\boldsymbol{\rho}(t) - \boldsymbol{\rho}^*(t)|| \quad , \quad e_v = \max_{t \in [0 \text{ TOF}]} ||\dot{\boldsymbol{\rho}}(t) - \dot{\boldsymbol{\rho}}^*(t)|| \tag{23}$$

Copyright © 2023 Advanced Maui Optical and Space Surveillance Technologies Conference (AMOS) – www.amostech.com

where e_p and e_v denote the maximum position and velocity errors over the time interval. In Equation 23, starred quantities deonte the truth values stemming from the nonlinear dynamics whereas the unmarked quantities are the results obtained from the linearized relative motion model. In Figure 4, the linearized equations of motion are validated along the 9:2 L_2 Near Rectilinear Halo Orbit (NRHO) in the BCRFBP. In the leftmost plot, the reference orbit is depicted with $\Psi_{T,0}$ indicating the where the target mean anomaly is 0° at perilune. Then, three color contour maps characterize the accuracy of linearized equations as a function of the target spacecraft's initial position. The center-left contour plot quantifies the chaser's initial relative distance as a function of Ψ_T vs $\Delta\Psi$. Note that if $\Delta\Psi > 0$, the fictitious chaser spacecraft is initialized *ahead* of the target along its $+\hat{\mathbf{i}}$ direction. Similarly, if $\Delta\Psi < 0$, the chaser is initialized *behind* the target along its $-\hat{\mathbf{i}}$ direction. The middle-right and far-right contour plots show the resulting position and velocity errors, respectively, from the propagation of the linearized relative motion models. All the color-coded information from each contour plot is placed on a log scale for convenience. Figure 5 plots the same information for the 3:1 L_1 Northern Halo reference orbit. Results from both cases indicate that the linearized equations of relative motion are most accurate near apolune where the relative velocities between spacecraft are minimized since the gravitational acceleration due to the closest primary, the Moon, is at a minimum. Consequently, this suggests that proximity operations between the target and chaser spacecraft should be initiated when the target's mean anomaly is between 150° to 210°. Although proximity operations can be designed and evaluated at any point along the reference orbits, the linearized equations of motion are most accurate when the target is near apolune. For this reason, NASA's proposed proximity operations between Gateway and Orion baselines rendezvous maneuvers to occur when both spacecraft are near apolune along the NRHO.

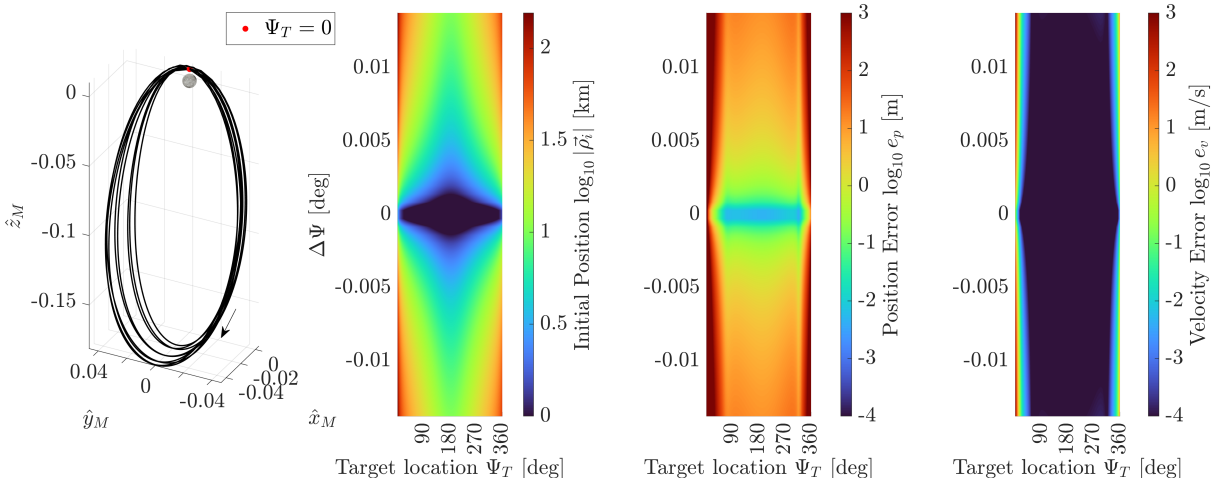

Fig. 4: Validation of linearized model on a 9:2 L_2 Near Rectilinear Halo Orbit (NRHO) in the BCRFBP. In the far-left plot, the target reference orbit is plotted along with the $\Psi_{T,0}$ point indicated in red. Each color contour plot contains information regarding the chaser's initial relative distance to the target (center-left), final position error (center-right), and final velocity error (far-right) resulting from the linearized equations of motion as a function of Ψ_T and $\Delta\Psi$ with a propagation time of 6.5 days.

Copyright © 2023 Advanced Maui Optical and Space Surveillance Technologies Conference (AMOS) – www.amostech.com

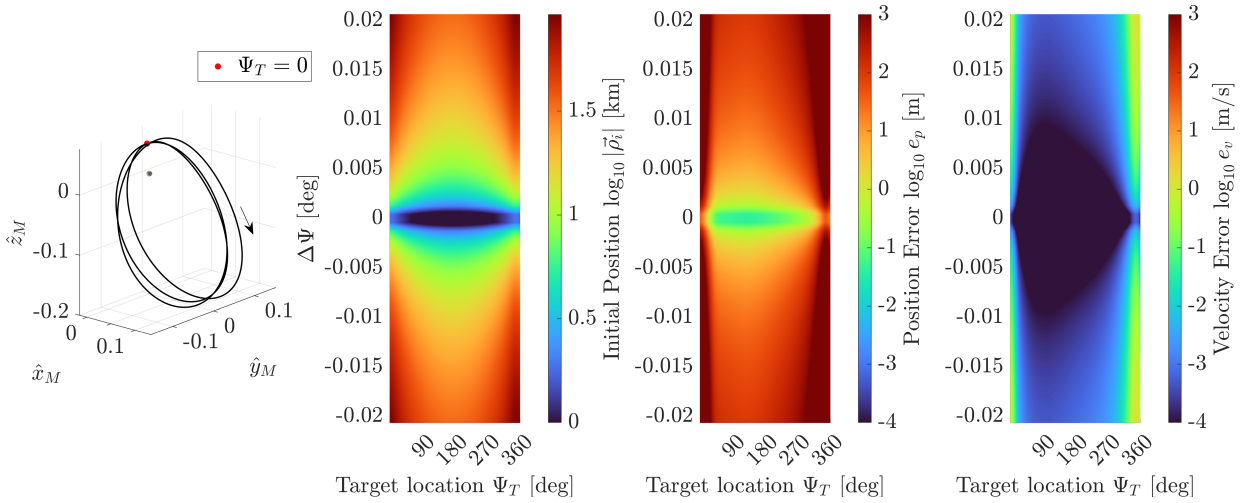

Fig. 5: Validation of linearized model on a 3:1 L_1 Northern Halo Orbit in the BCRFBP. In the far-left plot, the target reference orbit is plotted along with the $\Psi_{T,0}$ point indicated in red. Each color contour plot contains information regarding the chaser's initial relative distance to the target (center-left), final position error (center-right), and final velocity error (far-right) resulting from the linearized equations of motion as a function of Ψ_T and $\Delta\Psi$ with a propagation time of 9 days.

3. RENDEZVOUS & PROXIMITY OPERATIONS MISSION DESIGN

As indicated in the previous section, the accuracy of the linearized equations of relative motion can be leveraged for relative guidance and control applications including mission design for proximity operations. Since the relative equations characterize the chaser's relative state in the target spacecraft's LVLH frame, path planning can be performed with consideration to the target's local geometry. Assume that the chaser's relative position and velocity vectors, $\boldsymbol{\rho}$ and $[\dot{\boldsymbol{\rho}}(t)]_T$, respectively, can be expressed in component-wise form as

$$\boldsymbol{\rho} = [\imath\ ;\ \jmath\ ;\ \mathrm{k}] = \imath\hat{\mathbf{i}} + \jmath\hat{\mathbf{j}} + \mathrm{k}\hat{\mathbf{k}} \qquad [\dot{\boldsymbol{\rho}}]_T = [\mathrm{i}\ ;\ \mathrm{j}\ ;\ \dot{\mathrm{k}}] = \mathrm{i}\hat{\mathbf{i}} + \mathrm{j}\hat{\mathbf{j}} + \dot{\mathrm{k}}\hat{\mathbf{k}} \tag{24}$$

where $\hat{\mathbf{i}}$, $\hat{\mathbf{j}}$, and $\hat{\mathbf{k}}$ are the axes associated with the target's LVLH frame T. To leverage the linear relative motion models for guidance and control applications, the equations of motion can be written in state-space form such that

$$\dot{\boldsymbol{x}}(t) = \mathbf{A}(t)\boldsymbol{x}(t) + \mathbf{B}\boldsymbol{u}(t) \tag{25}$$

where $\boldsymbol{x}(t) \in \mathcal{R}^6$, $\mathbf{A}(t) \in \mathcal{R}^{6\times6}$, $\mathbf{B}(t) \in \mathcal{R}^{6\times3}$, and $\boldsymbol{u}(t)$ is the control vector representing the chaser's applied maneuvers in the target spacecraft's LVLH frame. Specifically,

$$\boldsymbol{x}(t) = \begin{bmatrix} \boldsymbol{\rho}(t) \\ [\dot{\boldsymbol{\rho}}(t)]_T \end{bmatrix} \qquad \mathbf{B} = \begin{bmatrix} \mathbf{0}_{3\times3} \\ \mathbf{I}_{3\times3} \end{bmatrix}$$

The system matrix $\mathbf{A}(t)$ is defined such that

$$\mathbf{A}(t) = \begin{bmatrix} \mathbf{0}_{3\times3} & \mathbf{I}_{3\times3} \\ \mathbf{A}_{\boldsymbol{\rho}\dot{\boldsymbol{\rho}}}(t) & -2\boldsymbol{\Omega}_{T/I}(t) \end{bmatrix}$$

Copyright © 2023 Advanced Maui Optical and Space Surveillance Technologies Conference (AMOS) – www.amostech.com

where the system matrix subcomponent, $\mathbf{A}_{\rho\dot{\rho}}(t)$, is evaluated at time t and expressed as

$$\mathbf{A}_{\rho\dot{\rho}}(t) = -[\underset{T}{\dot{\mathbf{\Omega}}_{T/I}}] - \mathbf{\Omega}_{T/I}^2 - \frac{\mu}{r^3}\left(\mathbf{I} - 3\frac{\boldsymbol{r}\boldsymbol{r}^T}{r^2}\right) - \frac{1-\mu}{||\boldsymbol{r}+\boldsymbol{r}_{em}||^3}\left(\mathbf{I} - 3\frac{(\boldsymbol{r}+\boldsymbol{r}_{em})(\boldsymbol{r}+\boldsymbol{r}_{em})^T}{||\boldsymbol{r}+\boldsymbol{r}_{em}||^2}\right) - \frac{\mu_s}{||\boldsymbol{r}+\boldsymbol{r}_{sm}||^3}\left(\mathbf{I} - 3\frac{(\boldsymbol{r}+\boldsymbol{r}_{sm})(\boldsymbol{r}+\boldsymbol{r}_{sm})^T}{||\boldsymbol{r}+\boldsymbol{r}_{sm}||^2}\right) \tag{26}$$

Khoury & Lippe[10] demonstrated that the evaluation of the system matrix $\mathbf{A}(t)$ can be used to numerically integrate the relative state transition matrix (STM) given by the relationship, $\dot{\mathbf{\Phi}}(t,t_0) = \mathbf{A}(t)\mathbf{\Phi}(t,t_0)$. Elements of the relative STM, which relate variations in the initial relative state at t_0 to the resulting relative state at time t, are used to formulate multiple shooting algorithms as a part of a differential corrections scheme in the target's LVLH frame T. A general overview of multiple shooting strategies in the CRTBP can be found in Grebow.[8] Moreover, examples using multiple shooting strategies for the relative equations of motion in the CRTBP can be found in Khoury.[11] Through the application of these shooting methods, chaser trajectories can be computed to adhere to desired geometries relative to the target spacecraft.

3.1 Proximity Operations along a 9:2 L_2 NRHO

In this scenario, proximity operations between a target and chaser spacecraft are demonstrated along a 9:2 L_2 NRHO. First, the chaser spacecraft is initialized 2 km *behind* the target along the reference NRHO. Then, the chaser proceeds to perform eight maneuvers, computed using a multiple shooting scheme, to approach the target and achieve terminal rendezvous at the end of the specified time period of 54 hours. The chaser's maneuvers are designed and implemented to produce a relative trajectory that continuously approaches the target spacecraft along its line-of-site (LOS) vector to the Sun. In Figure 6(a), the orbits of both the target (red) and chaser (blue) spacecraft along the 9:2 L_2 NRHO are shown in the Moon-centered Earth-Moon rotating frame M. Moreover, a projection of the Sun's position in the BCRFBP is also plotted relative to the Moon. In Figure 6(b), the chaser's trajectory relative to the target's LVLH frame is shown with the target's LOS vector geometry to the Sun. Finally, in Figure 6(c), the chaser's relative trajectory is resolved in a target centered frame fixed along the target's LOS vector to the Sun. In this plot, $\hat{\odot}$ is directed along the target's LOS vector to the Sun and $\hat{\mathbf{k}}$ is the target's radial vector to the Moon. The results of this scenario demonstrate the capability to produce chaser trajectories that adhere to a specific solar geometry relative to the target spacecraft. As outlined in Abell et al,[1] a potential application of this proximity operations demonstration along the 9:2 L_2 NRHO includes Orion-Gateway rendezvous operations which stipulate that Orion be positioned between Gateway and the Sun during the close range phase of the RPOD (Rendezvous, Proximity Operations, and Docking) concept of operations.

Copyright © 2023 Advanced Maui Optical and Space Surveillance Technologies Conference (AMOS) – www.amostech.com

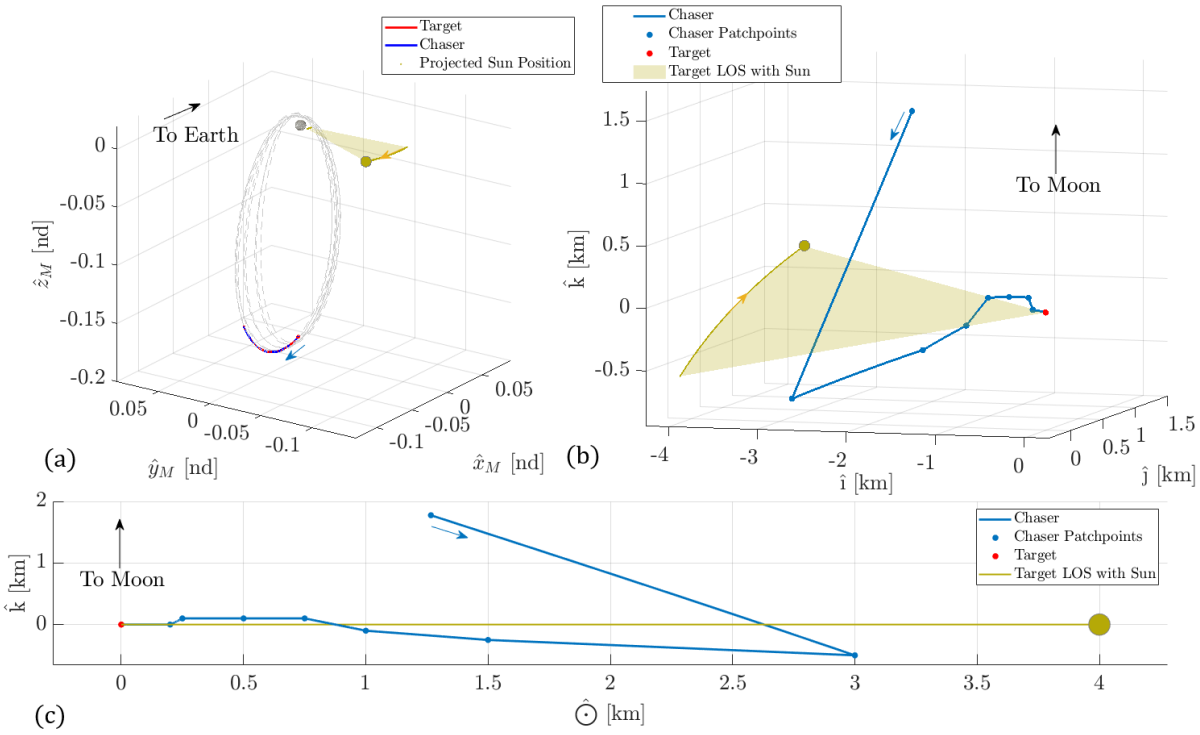

Fig. 6: Rendezvous scenario using a target-chaser configuration along a 9:2 L_2 NRHO: (a) The target (red) and chaser (blue) spacecraft are shown along the NRHO reference orbit in the Moon-centered Earth-Moon rotating frame. (b) The chaser's relative trajectory in the target's LVLH frame. (c) The same relative trajectory is resolved in a target-centered frame fixed along the target's LOS vector to the Sun.

3.2 Proximity Operations along a 3:1 L_1 southern halo orbit

One potential aspect of maintaining a permanent crewed presence on the Moon includes the establishment of fuel depots in the cislunar vicinity. Based on analyses from an internal NASA study in 2011,[5] it was assessed that the use of fuel depots would result in significant cost savings and reductions in launch mass compared to government-developed heavy lift rocket systems. These fuel depots can be used to refuel spacecraft that aim to access higher energy orbits or seek a return to Earth. Consequently, this work includes an investigation of proximity operations in a target-chaser configuration where the target spacecraft is a fuel depot structure flying along a 3:1 L_1 halo orbit. In this section, strategies are leveraged to insert the chaser spacecraft along the target's cislunar orbit from an Earth parking orbit to rendezvous with the target spacecraft during favorable lighting conditions. The resulting solution demonstrates a feasible low-cost lunar transfer design from Low Earth Orbit (LEO) to terminal rendezvous with a fuel depot residing in the cislunar vicinity.

3.2.1 Ballistic Lunar Transfer to L_1 halo

Ballistic Lunar Transfer options to L_1 halo orbits are constructed by leveraging dynamical structures within the BCR4BP model. For this example, the selected 3:1 L_1 halo orbit is depicted in Figure 2(a). The desired BLT option assumes a maneuver is performed at the arrival location on the

Copyright © 2023 Advanced Maui Optical and Space Surveillance Technologies Conference (AMOS) – www.amostech.com

desired L_1 halo orbit. To explore the options available, a Poincaré map is constructed by applying a tangential maneuver along a range of positions on the L_1 destination orbit and propagating in negative time towards the Earth. The destination L_1 halo is divided into 5418 potential insertion locations, recall that the 3:1 orbit selected has three revolutions. A maneuver with a magnitude of 210 m/s is applied in a direction opposite of the motion, i.e., opposite the velocity vector, at each halo insertion location. After the maneuver is applied, the trajectory is propagated in negative time with a maximum propagation time of a year (365 days). The Poincaré map in Fig. 7(a) is generated by collecting the first three periapsis states of each backwards propagated trajectory. Figure 7(a) depicts the generated map with a normalized τ parameter (range of $[0, 1]$) that represents the insertion location along the 3:1 halo orbit, note that $\tau = 0, 1$ corresponds to the same state along the periodic orbit. Next, the time-of-flight, TOF, is displayed on the y-axis of the generated map. Finally, each point on the map is assigned a color that corresponds to the distance from the Earth at the end of the propagation time corresponding to the first three identified periapsis states measured relative to Earth. An initial guess is selected from the map in Fig. 7(a), see the red circle, and plotted in Fig. 7(b). Observe that the selected initial transfer guess implements a single insertion maneuver at the arrival location on the L_1 halo. The selected initial guess is corrected via a multiple-shooting method with a Newton-Raphson algorithm and optimized, via MATLAB's FMINCON function, to decrease the insertion ΔV. The launch state, near the Earth, is constrained to be a periapsis, with respect to the Earth, and has an altitude of 200 km. Note that the Transfer Launch Injection (TLI) maneuver is not considered because it is assumed that the upper stage of the selected launch vehicle will provide the required energy to inject the spacecraft onto the BLT transfer. The ΔV optimized transfer to the desired 3:1 L_1 halo is presented in Fig 8 with an insertion maneuver of 93.36 m/s.

3.2.2 Rendezvous along L_1 halo

Dynamical structures in a BCR4BP model facilitate the construction of preliminary end-to-end rendezvous mission trajectories. A comprehensive rendezvous mission design consists of a transfer, e.g., typically from launch, and a close-proximity rendezvous operations trajectory. In this investigation, ballistic lunar transfers (BLTs) are explored as transfer options to deliver a chaser spacecraft to the vicinity of a destination orbit. The utilization of the BCRFBP model for the Earth-Moon system offers an additional advantage in the tracking of the Sun's position as a function of elapsed time since the initial epoch. As a result, the chaser spacecraft's close approach to the target can be designed to adhere to visibility constraints where the chaser maneuvers between the target and Sun to ensure favorable lighting conditions for its onboard cameras and tracking sensors. As observed in Figure 9(a), the orbits of both the target (red) and chaser (blue) spacecraft along the 3:1 L_1 halo orbit are shown in the Moon-centered Earth-Moon rotating frame with a projection of the Sun's position over time. In Figure 9(b), the chaser's trajectory relative to the target's LVLH frame is shown with the target's LOS vector to the Sun. Finally, in Figure 9(c), the chaser's relative trajectory is resolved in a target centered frame fixed along the target's LOS vector to the Sun. In this plot, $\hat{\odot}$ is directed along the target's LOS vector to the Sun and $\hat{\mathbf{k}}$ is the target's radial vector to the Moon. In this scenario, the chaser initially begins its close approach along the target's LOS vector to the Sun but then proceeds to perform four maneuvers to fly around the target spacecraft to simulate a final inspection procedure prior to the final intercept trajectory.

Copyright © 2023 Advanced Maui Optical and Space Surveillance Technologies Conference (AMOS) – www.amostech.com

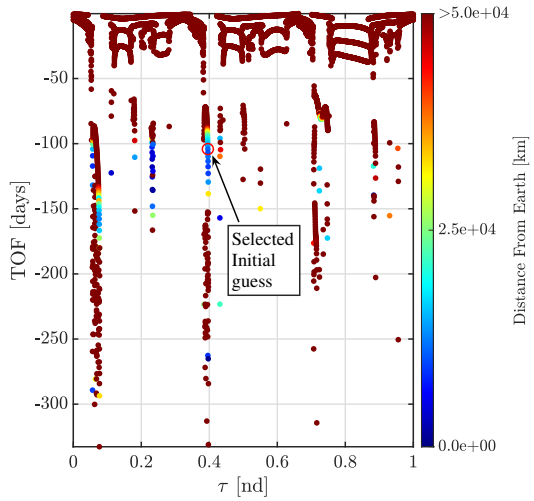

(a)

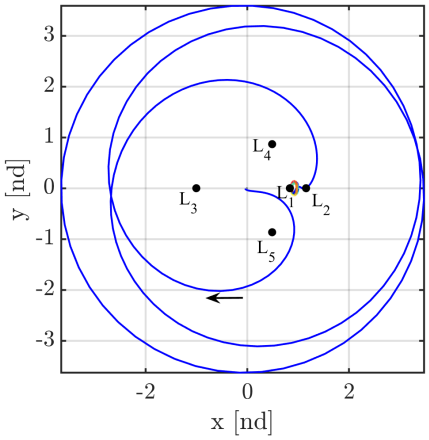

(b)

Fig. 7: (a) Poincaré map of trajectories propagated in negative from insertion positions along the desired 3:1 halo orbit. A selected initial guess is displayed as a red circle (b) Selected initial trajectory guess generated from map in the Earth-Moon rotating frame of the BCR4BP model. Note that the axis are non-dimensionalized with the l^* value.

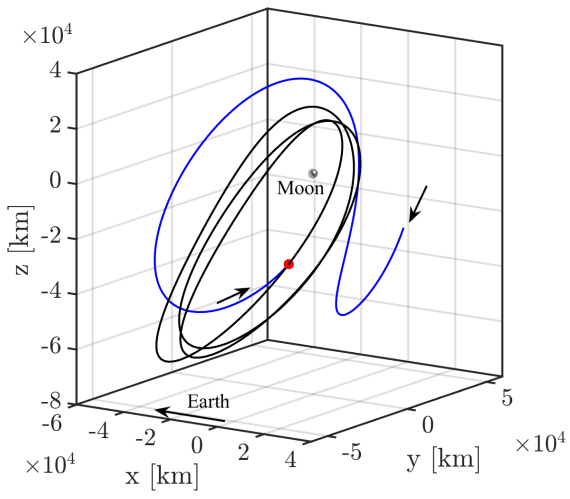

(a)

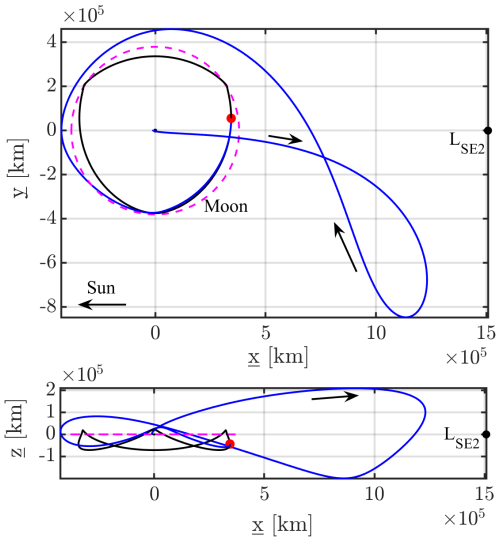

(b)

Fig. 8: (a) Optimal BLT to the desired 3:1 halo orbit in the Moon-Centered Earth-Moon rotating frame of the BCR4BP. The red point corresponds to the maneuver location to insert into the halo orbit. (b) B_1-Centered Sun-B_1 frame of the BCR4BP model representation of the optimal transfer. The moon is depicted as a dashed magenta line.

Copyright © 2023 Advanced Maui Optical and Space Surveillance Technologies Conference (AMOS) – www.amostech.com

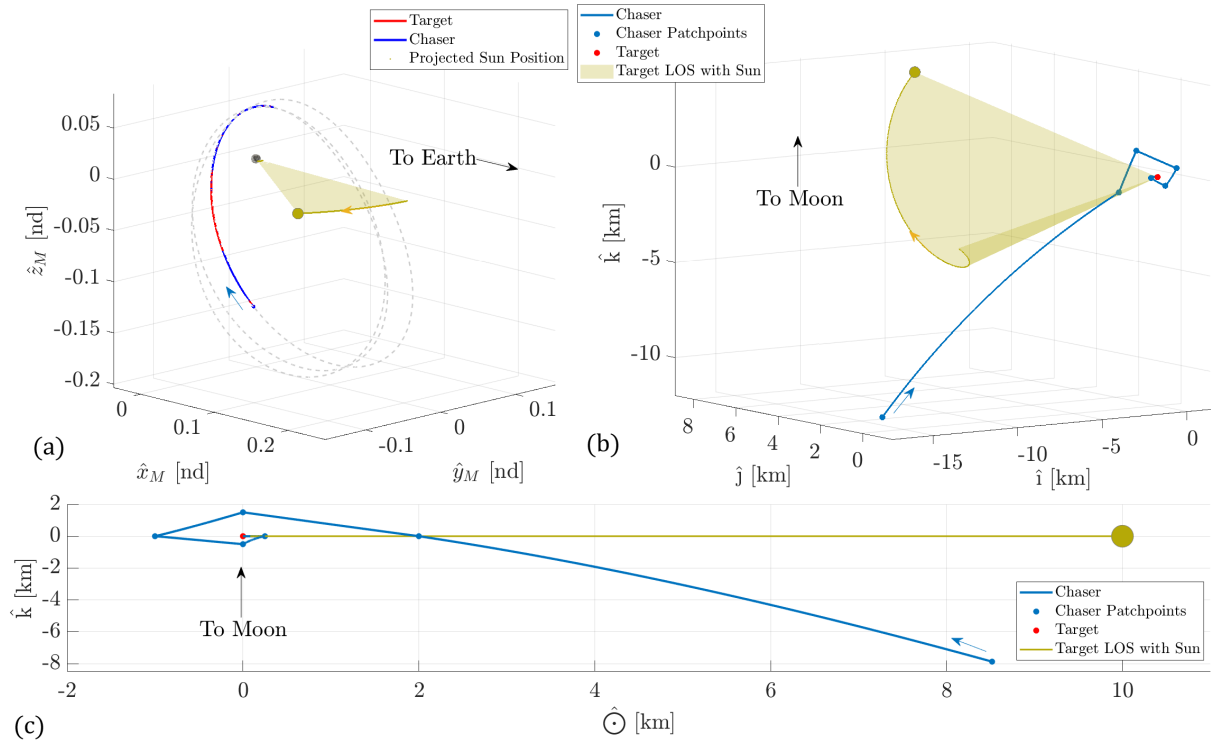

Fig. 9: Rendezvous scenario using a target-chaser configuration along a 3:1 L_1 southern halo orbit. In the top left plot, the target (red) and chaser (blue) spacecraft are shown along the halo reference orbit in the Moon-centered Earth-Moon rotating frame. The chaser's relative trajectory in the target's LVLH frame is shown in the top right plot. The same relative trajectory is resolved in a target-centered frame fixed along the target's LOS vector to the Sun (bottom plot).

Results for the converged rendezvous trajectories along both the 9:2 L_2 NRHO and 3:1 L_1 halo orbit are provided in Table 1. They include the total number and cost of maneuvers associated with each rendezvous profile in addition to the number of iterations produced to converge each rendezvous trajectory. In both cases, a time of flight (TOF) between 2-3 days was considered for consistency with the proposed timeline for rendezvous between the Orion and Gateway. Moreover, by using the chaser spacecraft's nominal trajectory prior to rendezvous as an initial guess for the differential corrector, the final corrected trajectory converged within two iterations using the employed multiple shooting scheme.

Table 1: Mission profiles in the BCRFBP.

Target Orbit	*Total Number of Maneuvers*	*TOF*	Δv *Total*	*Iterations*
9:2 L_2 NRHO	8	54 hrs.	26.5 cm/s	2
3:1 L_1 Halo	5	60 hrs.	1.3 m/s	2

Copyright © 2023 Advanced Maui Optical and Space Surveillance Technologies Conference (AMOS) – www.amostech.com

4. CONCLUSION

As crewed space exploration expands past Earth orbit to the Moon, new technologies must be developed to facilitate the coordination of spacecraft in the cislunar dynamical environment. Orbits residing in the cislunar vicinity are governed simultaneously by the gravitational influence of both the Earth and the Moon. Conventional methods for relative spacecraft GNC are designed for proximity operations in Earth orbit and subsequently fail to accurately characterize the relative motion between spacecraft in the Earth-Moon system. The few relative dynamics models that incorporate Earth and Moon gravity do not include the nontrivial effects of the Sun on orbits in the cislunar vicinity. The Sun imparts an additional gravitational acceleration on these orbits and dictates the necessary lighting conditions for close range proximity operations between spacecraft. To overcome limitations in conventional methods, this work leverages a dynamical framework which characterizes the relative dynamics between a target and chaser spacecraft in the context of the BCRFBP. As a result, numerical tools are developed to generate rendezvous trajectories in a local rotating frame attached to the target which adhere to Sun-lit geometries that guarantee visibility requirements during close approach. Two scenarios involving proximity operations along cislunar orbits are investigated including a 9:2 L_2 NRHO and a 3:1 L_1 halo orbit. In the NRHO case, a chaser spacecraft performs a sequence of maneuvers to achieve terminal rendezvous with a target spacecraft along the target's line of sight vector to the Sun. The resulting trajectory is modeled after the proposed concept of operations for the Orion spacecraft's RPOD with the Gateway orbiting platform. In the case involving the 3:1 L_1 halo orbit, a feasible mission design trajectory is obtained for a chaser spacecraft starting at LEO to achieve terminal rendezvous with a target representing the location of a cislunar fuel depot. A ballistic lunar transfer (BLT) is leveraged to produce a solution from an Earth parking orbit to insertion along the target's orbit followed by a sequence of maneuvers characterizing the chaser's close approach to the target. During the close approach, the chaser spacecraft circumnavigates the target spacecraft prior to rendezvous along its line of sight vector to the Sun. Both scenarios underscore the advantages of characterizing spacecraft relative dynamics in the BCRFBP and demonstrate new capabilities for proximity operations mission design along orbits in the cislunar dynamical environment.

REFERENCES

[1] Jordan S Abell, Peter Z Schulte, Fred D Clark, Peter T Spehar, and David C Woffinden. Orion gn&c sequencing for off-nominal rendezvous, proximity operations, and docking. In *31st AAS/AIAA Space Flight Mechanics Meeting, Charlotte, NC*, number AAS 21-439, 2021.

[2] Esther Barrabés, Gerard Gómez, Josep M Mondelo, and Mercé Ollè. Pseudo-heteroclinic connections between bicircular restricted four-body problems. *Monthly Notices of the Royal Astronomical Society*, 462(1):740–750, 2016.

[3] Kenza K Boudad. *Trajectory Design Between Cislunar Space and Sun-Earth Libration Points in a Four-Body Model*. PhD thesis, Purdue University Graduate School, 2022.

[4] Kenza K Boudad, Kathleen C Howell, and Diane C Davis. Dynamics of synodic resonant near rectilinear halo orbits in the bicircular four-body problem. *Advances in Space Research*, 66(9):2194–2214, 2020.

Copyright © 2023 Advanced Maui Optical and Space Surveillance Technologies Conference (AMOS) – www.amostech.com

[5] David Cheuvront. Propellant depot alternative drm 34b. Technical Report DRM-34B, NASA Johnson Space Center Safety and Mission Assurance Shuttle and Exploration Division, 2101 E NASA Pkwy, Houston, TX, Nov 2011.

[6] WH Clohessy and RS Wiltshire. Terminal guidance system for satellite rendezvous. *Journal of the aerospace sciences*, 27(9):653–658, 1960.

[7] Giovanni Franzini, Mario Innocenti, et al. Relative motion equations in the local-vertical local-horizon frame for rendezvous in lunar orbits. In *Proceedings of the 2017 Astrodynamics Conference, Advances in Astronautical Sciences*, volume 162, pages 2603–2617. American Astronautical Society, 2017.

[8] Daniel J Grebow. *Trajectory design in the Earth-Moon system and lunar South Pole coverage*. PhD thesis, Purdue University, 2010.

[9] Su-Shu Huang. Very restricted four-body problem. *Publications of Goddard Space Flight Center*, 354, 1960.

[10] F. Khoury and C. Lippe. Relative guidance, navigation, and control in mutibody gravitational regimes. In *2022 AAS/AIAA Astrodynamics Specialist Conference, Charlotte, NC, USA, Aug. 2022*, number Paper AAS 22-710, 2022.

[11] Fouad Khoury and Kathleen C Howell. Orbital rendezvous and spacecraft loitering in the earth-moon system. In *AAS/AIAA Astrodynamics Specialist Conference, Lake Tahoe, California, USA*, 2020.

[12] Brian P McCarthy and Kathleen C Howell. Cislunar transfer design exploiting periodic and quasi-periodic orbital structures in the four-body problem. In *71st International Astronautical Congress, Virtual*, 2020.

[13] Robert Pritchett, Kathleen C Howell, and David C Folta. Low-thrust trajectory design for a cislunar cubesat leveraging structures from the bicircular restricted four-body problem. In *70 International Astronautical Congress, Washington D.C.*, number GSFC-E-DAA-TN73884-1, 2019.

[14] Hanspeter Schaub. Relative orbit geometry through classical orbit element differences. *Journal of Guidance, Control, and Dynamics*, 27(5):839–848, 2004.

[15] Stephen Scheuerle Jr. *Construction of ballistic lunar transfers in the earth-moon-sun system*. PhD thesis, Purdue University Graduate School, 2021.

[16] Joshua Sullivan, Sebastian Grimberg, and Simone D'Amico. Comprehensive survey and assessment of spacecraft relative motion dynamics models. *Journal of Guidance, Control, and Dynamics*, 40(8):1837–1859, 2017.

[17] Victory Szebehely. *Theory of orbit: The restricted problem of three Bodies*. Elsevier, 2012.

[18] Koji Yamanaka and Finn Ankersen. New state transition matrix for relative motion on an arbitrary elliptical orbit. *Journal of guidance, control, and dynamics*, 25(1):60–66, 2002.

[19] Emily M Zimovan, Kathleen C Howell, and Diane C Davis. Near rectilinear halo orbits and their application in cis-lunar space. In *3rd IAA Conference on Dynamics and Control of Space Systems, Moscow, Russia*, volume 20, page 40, 2017.

Copyright © 2023 Advanced Maui Optical and Space Surveillance Technologies Conference (AMOS) – www.amostech.com